Letter

Hall viscosity and hydrodynamic inverse Nernst effect in graphene

Zhuo-Yu Xian [1], Sven Danz,[1,2,3] David Rodríguez Fernández,[1,4] Ioannis Matthaiakakis [1,5] Christian Tutschku,[1,6] Raffael L. Klees [1], Johanna Erdmenger,[1] René Meyer,[1] and Ewelina M. Hankiewicz[1]

[1]*Institute for Theoretical Physics and Astrophysics and Würzburg-Dresden Cluster of Excellence ct.qmat, Julius-Maximilians-Universität Würzburg, D-97074 Würzburg, Germany*
[2]*Peter Grünberg Institute - Quantum Computing Analytics (PGI 12), Forschungszentrum Jülich, D-52425 Jülich, Germany*
[3]*Theoretical Physics, Saarland University, D-66123 Saarbrücken, Germany*
[4]*Instituut-Lorentz for Theoretical Physics, Universiteit Leiden, P.O. Box 9506, NL-2300 RA Leiden, The Netherlands*
[5]*Dipartimento di Fisica, Università di Genova and I.N.F.N. - Sezione di Genova, via Dodecaneso 33, I-16146 Genova, Italy*
[6]*Fraunhofer IAO, Fraunhofer Institute for Industrial Engineering IAO, D-70569 Stuttgart, Germany*

Motivated by Hall viscosity measurements in graphene sheets, we study hydrodynamic transport of electrons in a channel of finite width in external electric and magnetic fields. We consider electric charge densities varying from close to the Dirac point up to the Fermi-liquid regime. We find two competing contributions to the hydrodynamic Hall and inverse Nernst signals that originate from the Hall viscous and Lorentz forces. This competition leads to a nonlinear dependence of the full signals on the magnetic field and even a cancellation at different critical field values for both signals. In particular, the hydrodynamic inverse Nernst signal in the Fermi-liquid regime is dominated by the Hall viscous contribution. We further show that a finite channel width leads to a suppression of the Lorenz ratio, while the magnetic field enhances this ratio. All of these effects are predicted in parameter regimes accessible in experiments.

Introduction. In the last two decades, electronic fluids have become a main research object in condensed matter physics, allowing for the realization of new transport effects. The main platform for electron hydrodynamics studies and applications is graphene [1–11], for which hydrodynamic behavior can be experimentally accessed both close to the Dirac point as well as in the Fermi-liquid regime [12–14]. In particular, graphene allows the investigation of new transport effects induced by the Hall viscosity η_H, which was recently measured to be of the same order of magnitude as the shear viscosity η [9] and thus strongly affects the hydrodynamic properties of graphene. More precisely, both η and η_H determine the transport properties of electronic fluids in finite sample geometries [3,4,15]. This was observed experimentally in GaAs [16–18], graphene [3,4,7,9], and PdCoO$_2$ compounds [1]. Moreover, the full ballistic-to-hydrodynamic crossover [16,17] as well as a negative magnetoresistance due to viscous effects [19–22] were observed in channel geometries.

The Hall viscosity η_H breaks parity and time-reversal symmetries [23–25], and is generated in a parity-invariant electronic fluid by an external magnetic field [9,20]. In GaAs Fermi liquids, there is a competition of the Hall viscous and Lorentz forces acting on the fluid [26]. In contrast, the relativistic Dirac spectrum in graphene enables new hydrodynamic transport effects.

In this Letter, we find different contributions to the thermoelectric transport of the electronic fluid in graphene in the presence of an external magnetic field. We predict that the hydrodynamic inverse Nernst effect consists of contributions stemming from the Lorentz and Hall viscous forces that arise both close to charge neutrality as well as in the Fermi-liquid regime. Moreover, close to the Dirac point [27], we find that the quantum critical (or incoherent) conductivity σ_Q [12,28], originating from momentum-conserving scattering between electrons and holes, crucially contributes to the hydrodynamic inverse Nernst signal as well. In addition, we show a cancellation between the Hall viscous and Lorentz force contributions in both the hydrodynamic Hall and inverse Nernst signals at different critical magnetic fields of the order of 10 mT. The critical fields increase with increasing μ/k_BT. Let us emphasize that our hydrodynamic inverse Nernst effect scales differently with the system size and out-of-plane magnetic field in comparison with Nernst/inverse Nernst effects in ballistic or diffusive regimes of metals, ferromagnets, and spin-orbit systems [29–31].

Finally, we calculate the thermal and electric conductivities and show their ratio violates the Wiedemann-Franz law [2,32,33]. We predict that the magnitude of the violation is a monotonically increasing function of both the external magnetic field and the width of the channel. We predict these effects based on our innovative theoretical approach involving a fully relativistic analysis, and implementing boundary conditions that include the fluid's thermodynamics.

Hydrodynamics in a graphene channel. We consider a graphene channel of width W and length $L \gg W$ subjected to an electric field $\boldsymbol{E} = E_x\boldsymbol{e}_x$ and a magnetic field $\boldsymbol{B} = B_z\boldsymbol{e}_z$ (see Fig. 1). The electrons with charge $-e$ are pumped through the channel by $\boldsymbol{E}$ and are deflected towards the channel boundaries by the Lorentz force density $\boldsymbol{f}_B$ and the Hall viscous force density $\boldsymbol{f}_{\eta_H}$ defined in Eqs. (2e) and (2f) below. The Hall viscous force density $\boldsymbol{f}_{\eta_H}$ is induced by the Hall viscosity
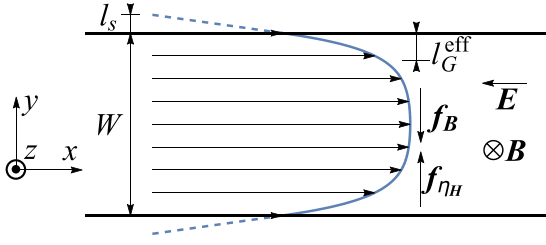
FIG. 1. Velocity profile of an electron fluid in a graphene channel of width W, with applied electric field $\boldsymbol{E}$ and magnetic field $\boldsymbol{B}$. l_s is the slip length and l_G^{eff} is the effective Gurzhi length. $\boldsymbol{f}_B$ and $\boldsymbol{f}_{\eta_H}$ are the Lorentz and Hall force densities, respectively.

η_H, defined in the Supplemental Material (SM) [34], which is a parity-breaking dissipationless transport coefficient in the hydrodynamic expansion of the stress tensor [23,24,35]. These forces trigger the transverse temperature gradient ΔT (inverse Nernst effect) and the Hall voltage ΔV across the channel [36]. To avoid excessive Joule heating and to stay in the linear response regime, we consider small electric fields. We consider $|B_z| \ll 1$ T to avoid the formation of Landau levels.

For the validity of electron hydrodynamics in the graphene channel, the electron fluid should reach local equilibrium via fast scattering compared to other effects, such as momentum relaxation, energy relaxation, and the effect of a finite channel width. We maintain the hierarchy between the corresponding characteristic times by considering reasonable parameters, such as $\mu/k_B T > 0.1$ and 100 K $< T < 300$ K (see SM [34] and Ref. [37]). Within this region, the electron-electron scattering characterized by the dimensionless coupling $\alpha \approx 0.5$ leads to the electron-electron scattering time $\tau_{ee} \sim 0.1$ ps [12]. The momentum relaxation time τ_{MR} and energy relaxation time τ_{ER} are of the order of 1 ps [8,28,38–40] and 100 ps [41–47], respectively, for our range of parameters. Finally, the "ballistic" time is $\tau_B \sim W/v_F$, where W is the width of the channel and $v_F \simeq 10^6$ m/s is the Fermi velocity in graphene [21]. To avoid ballistic effects, we consider a width of the order $W \sim 1$ μm for which $\tau_B \sim 1$ ps. For the range of parameters we consider (i) we are always in the hydrodynamic regime and (ii) momentum relaxation must be taken into account. Since τ_{ER} is much larger than all other timescales, neglecting energy relaxation does not lead to qualitative changes of our results.

The hydrodynamic fluid variables are the flow velocity $\boldsymbol{v}$, the electrochemical potential μ_{tot}, and the total temperature T_{tot}. At global equilibrium and vanishing external sources, these are the usual velocity, chemical potential, and temperature characterizing a thermal state. This changes when external sources are turned on. In particular, within linear response, a nonzero electric field E_x and temperature gradient $\nabla_x T$ can be incorporated into μ_{tot} and T_{tot}. Thus, we consider small fluctuations $(\delta\mu, \delta T, v_x, v_y)$ around the global equilibrium at zero velocity, constant chemical potential μ, and temperature T,

$$\boldsymbol{v} = (v_x(y), v_y(y)), \tag{1a}$$

$$\mu_{\text{tot}} = \mu + \delta\mu(y) + exE_x, \tag{1b}$$

$$T_{\text{tot}} = T + \delta T(y) + x\nabla_x T. \tag{1c}$$

Linear response requires $\delta\mu \ll \mu$ and $\delta T \ll T$. The x-translation invariance along the channel implies the fluctuation fields can depend only on y. $\delta\mu$ can be further split into two contributions as $\delta\mu(y) = \delta\mu_T(y) - e\phi_V(y)$, where $\delta\mu_T$ is the deviation from thermal equilibrium and ϕ_V is the Vlasov potential generated by the backreaction of the fluid on the electric field [13,20,48].

Due to the relativistic dispersion relation of graphene, the hydrodynamic variables are fixed by relativistic hydrodynamics at linear order in the velocities [24,49–51], with a limit velocity v_F and an effective electrical field $(c/v_F)\boldsymbol{E}$. Following Eq. (1), the hydrodynamic equations read [34]

$$w\partial_y v_y = wv_y' = 0, \tag{2a}$$

$$enE_1 - \eta v_x'' - \boldsymbol{f}_{\eta_H,x} = -\frac{P_x}{\tau_{\text{MR}} v_F^2} + \boldsymbol{f}_{B,x}, \tag{2b}$$

$$\delta p' - \boldsymbol{f}_{\eta_H,y} - \eta v_y'' - en\phi_V' = -\frac{P_y}{\tau_{\text{MR}} v_F^2} + \boldsymbol{f}_{B,y}, \tag{2c}$$

$$\partial_y J_y = 0, \tag{2d}$$

$$\boldsymbol{f}_B = \frac{1}{n}\epsilon^{ij}\boldsymbol{e}_i J_j B_z, \tag{2e}$$

$$\boldsymbol{f}_{\eta_H} = \frac{\eta_H}{n}\epsilon^{ij}\boldsymbol{e}_i v_j''. \tag{2f}$$

Equations (2a)–(2d) correspond to the conservation of energy, longitudinal momentum, transversal momentum, and charge, respectively. The transport coefficients η and η_H are the shear and Hall viscosities, which are both positive in our setup (see Fig. S2 of the SM [34]). Moreover, n, n_E, p, w, and s are the equilibrium particle number density, energy density, pressure, enthalpy, and entropy density, respectively. They are all known functions of μ and T satisfying $w = n_E + p = 3n_E/2 = \mu_T n + sT$ [34]. The deviation of the pressure away from equilibrium is related to the hydrodynamic variables by $\delta p = n\delta\mu_T + s\delta T$. A central ingredient of our analysis is that the Lorentz force density $\boldsymbol{f}_B$ and the Hall viscous force density $\boldsymbol{f}_{\eta_H}$ have opposite signs. The relative and overall signs of the force densities stem from the following considerations: The origin of the relative sign is the opposite signs of the Poiseuille flow, $v_x > 0$, and its curvature, $v_x''(y) < 0$, in the coordinate system of Fig. 1. The overall sign is set by eB_z, which enters both force densities in the same way. The forces point in exactly opposite directions since the dominant v_x and v_x'' generate $\boldsymbol{f}_B$ and $\boldsymbol{f}_{\eta_H}$, respectively. These forces are in turn responsible for creating the velocity profile v_y, whose magnitude is much smaller than v_x, $|v_x| \gg |v_y|$. To summarize, the antiparallel configuration of the forces gives rise to the unconventional thermoelectric response we find below.

The charge currents $J_{x,y}$ and momenta $P_{x,y}$ entering the conservation equations (2) are

$$J_x = -env_x + \sigma_Q(B_z v_y + E_2), \tag{3a}$$

$$J_y = -env_y + \sigma_Q\left[-B_z v_x + \frac{1}{e}\left(\delta\mu' - \frac{\mu}{T}\delta T'\right)\right], \tag{3b}$$

$$P_x = wv_x, \quad P_y = wv_y. \tag{3c}$$

To simplify notation, we have recombined the sources into $E_1 = E_x + s\nabla_x T/(en)$ and $E_2 = E_x - \mu\nabla_x T/(eT)$. From Eq. (3), we see that E_1 drives the momentum density P_x and E_2 the quantum critical current density $J_Q = \sigma_Q E_2$. In principle, we should also consider the electrostatic Poisson equation to calculate the Vlasov field and close our system of equations. However, since the problem is linear, we can combine ϕ'_V and $\delta\mu'_T$ to $\delta\mu'$ in Eq. (2c) and solve Eq. (2) for the variables v_x, v_y, $\delta\mu$, and δT. Note that the above considerations are valid for an electron-dominated flow. A hole-dominated one is obtained by replacing $e \to -e$ and $\eta_H \to -\eta_H$ in Eqs. (2b) and (2c) [19,52]. In this case, both the Lorentz and Hall viscous forces change signs but the relative sign is preserved, leading only to an overall opposite Hall signal.

The transport coefficients σ_Q, η, and η_H are known functions of $\mu/k_B T$ and B_z [48,52,53] (see also SM [34]). Their most important features pertinent to our analysis are that η and η_H decrease for increasing $|B_z|$, while σ_Q decreases with increasing $\mu/k_B T$.

Finally, we fix the boundary conditions of $\boldsymbol{v}$ by requiring a vanishing current outflow in the y direction and a finite current along the channel boundaries. That is,

$$v_x(\pm W/2) \pm l_s v'_x(\pm W/2) = v_y(\pm W/2) = 0, \qquad (4)$$

with the slip length l_s (cf. Fig. 1) parametrizing the diffusivity of the channel [54]. The boundary conditions for $\delta\mu$ and δT are fixed through the conservation of the total charge and energy within the channel, which implies $\int_{-W/2}^{W/2} dy\,\delta n = 0 = \int_{-W/2}^{W/2} dy\,\delta n_E$.

Inserting Eq. (4) in Eqs. (2a) and (2d), one finds $J_y = P_y = v_y = 0$. With this, the velocity profile reads

$$v_x = -\frac{enE_1 l_G^{\text{eff}2}}{\eta}\left(1 - \frac{l_G^{\text{eff}}\cosh\frac{y}{l_G}}{l_G \sinh\frac{W}{2l_G}}\right), \qquad (5)$$

while $\delta\mu$ and δT are presented in the SM [34]. We have defined the Gurzhi length $l_G = v_F\sqrt{\eta\tau_{\text{MR}}/w}$ [12,55–57] and the effective Gurzhi length $l_G^{\text{eff}} = l_G[\coth(W/2l_G) + l_s/l_G]^{-1}$, which takes into account the effect of the channel geometry and the slip length on the flow. As sketched in Fig. 1, l_G^{eff} reflects the effective segmentation of the channel of width W into two boundary segments of width l_G^{eff} and an interior segment of width $W - 2l_G^{\text{eff}}$. For our range of parameters $l_G > 0.5$ μm at $B_z = 0$ and l_G decreases as B_z increases.

Some comments on v_x are in order: At $B_z = 0$, $l_{ee} < W < l_G$, the system is in the Poiseuille regime and v_x exhibits a parabolic dependence on y. Due to the large curvature of the flow, the Hall viscous effect becomes more important in this regime, as seen from Eq. (2c). When we increase the magnitude of B_z, the Gurzhi length l_G decreases and drives the system into the porous region $l_{ee} < l_G < W$ [3]. The velocity v_x then exhibits a plateau with a maximum $v_{x,\text{max}} = -enE_1 v_F^2\tau_{\text{MR}}/w$ in the interior of the channel [34], rendering the Hall viscous effect negligible.

We now draw our attention to the generalized Ohm's law for the conductivity matrix. Substituting Eq. (5) into Eq. (3)

and imposing $J_y = P_y = v_y = 0$, we obtain the average charge and heat currents along the channel,

$$\begin{pmatrix} J_x^{\text{avg}} \\ Q_x^{\text{avg}} \end{pmatrix} = \int \frac{dy}{W}\begin{pmatrix} J_x \\ Q_x \end{pmatrix} = \begin{pmatrix} \sigma & \alpha \\ \bar{\alpha}T & \bar{\kappa} \end{pmatrix}\begin{pmatrix} E_x \\ -\nabla_x T \end{pmatrix},$$

$$\begin{pmatrix} \sigma & \alpha \\ \bar{\alpha}T & \bar{\kappa} \end{pmatrix} = \begin{pmatrix} \sigma_Q + \frac{e^2 n^2 v_F^2}{w}\tau_{\text{MR}}^{\text{avg}} & \frac{\mu\sigma_Q}{eT} - \frac{ensv_F^2}{w}\tau_{\text{MR}}^{\text{avg}} \\ \frac{\mu\sigma_Q}{e} - \frac{ensTv_F^2}{w}\tau_{\text{MR}}^{\text{avg}} & \frac{\mu^2\sigma_Q}{e^2T} + \frac{s^2Tv_F^2}{w}\tau_{\text{MR}}^{\text{avg}} \end{pmatrix}, \qquad (6)$$

with the heat current $Q_x = P_x v_F - \mu J_x/(-e)$, the electrical conductivity σ, the thermoelectric conductivities α and $\bar{\alpha}$, and the thermal conductivity $\bar{\kappa}$. We have also defined the average momentum relaxation time $\tau_{\text{MR}}^{\text{avg}} = \tau_{\text{MR}}(1 - 2l_G^{\text{eff}}/W)$, which showcases the effect of finite boundaries on momentum relaxation. We note that $0 < \tau_{\text{MR}}^{\text{avg}} \leqslant \tau_{\text{MR}}$ holds for finite W, l_G, l_s. In the SM [34], we show that Eq. (6) agrees with the Onsager relation in the boundaryless limit $W \to \infty$ [50,58].

Hall voltage and hydrodynamic inverse Nernst effect. Given the solution for $\delta\mu$ and δT, we can calculate explicitly both the total Hall voltage ΔV and temperature gradient ΔT across the channel. Furthermore, the linear response assumption allows us to split both into two contributions: one due to the Lorentz force, ΔV_B and ΔT_B, and another one due to η_H and the Hall viscous force, ΔV_{η_H} and ΔT_{η_H}. Namely, $\Delta V = [\delta\mu(W/2) - \delta\mu(-W/2)]/(-e) = \Delta V_B + \Delta V_{\eta_H}$, where

$$\Delta V_B = -\frac{WB_z}{ew}\left(e^2 n v_F^2\tau_{\text{MR}}^{\text{avg}}E_1 + \mu\sigma_Q E_2\right),$$

$$\Delta V_{\eta_H} = -\frac{2\mu n\eta_H l_G^{\text{eff}}}{\eta w}E_1, \qquad (7)$$

and $\Delta T = \delta T(W/2) - \delta T(-W/2) = \Delta T_B + \Delta T_{\eta_H}$, where

$$\Delta T_B = \frac{WB_z T\sigma_Q}{w}E_2, \quad \Delta T_{\eta_H} = \frac{2enT\eta_H l_G^{\text{eff}}}{\eta w}E_1. \qquad (8)$$

The decomposition in Eq. (7) showcases that the Hall viscous voltage ΔV_{η_H} is generated from the curvature of the flow within the two boundary segments of size l_G^{eff}. In contrast, $\Delta V_B = -WB_z J_x^{\text{avg}}$ takes the traditional form expected from the Hall effect. In our case, the current is given by Eq. (6) and contains two contributions: one from the quantum critical conductivity σ_Q and another one from a Drude conductivity proportional to $\tau_{\text{MR}}^{\text{avg}}$ and renormalized by the finite channel width and shear viscosity. Remarkably, ΔT_B does not receive a contribution from momentum relaxation due to the vanishing momentum density in the y direction [cf. Eq. (6)].

Most notably for electrons, $\text{sgn}(\eta_H) = -\text{sgn}(B_z)$ results in ΔV_B (ΔT_B) and ΔV_{η_H} (ΔT_{η_H}) having opposite sign. Thus, the total Hall voltage or temperature gradient can become zero if the two contributions become equal. We can see from their ratio $\Delta V_{\eta_H}/\Delta V_B$ and $\Delta T_{\eta_H}/\Delta T_B$ at $\nabla_x T = 0$ (i.e., $E_{1,2} = E_x$) that both are comparable to unity only for small l_s, W, and B_z, which restricts ourselves to $l_s \ll W \sim 1$ μm. For increasing l_s, W, and B_z, the velocity v_x becomes flatter and as a result the force induced by η_H becomes smaller. Hence, while ΔV_{η_H} and ΔT_{η_H} saturate according to Eqs. (7) and (8), $|\Delta V_B|$ and $|\Delta T_B|$ keep growing with increasing $|B_z|$ and, eventually, ΔV and ΔT are dominated by ΔV_B and ΔT_B, respectively.
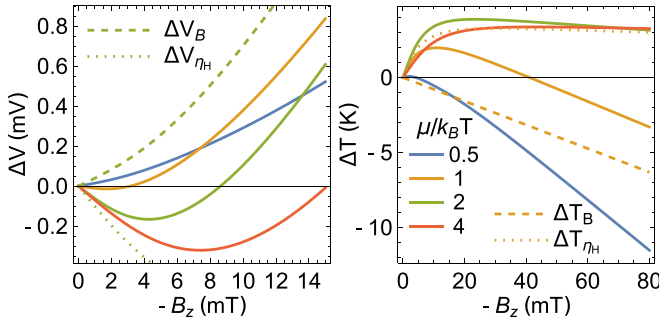
FIG. 2. Hall voltage ΔV and temperature gradient ΔT as functions of the magnetic field B_z. The other parameters are $T = 120$ K, $E_x = -1000$ V/m, $\nabla_x T = 0$, $W = 2$ μm. The dashed (dotted) lines show ΔV_B (ΔV_{η_H}) for $\mu = 2k_B T$ and ΔT_B (ΔT_{η_H}) for $\mu = k_B T$.

This leads to the *nonmonotonic* behavior in Fig. 2 and in particular to a zero of both ΔV and ΔT at certain finite B_z. Note that the nonmonotonic behavior appears only in the regime $\mu \gtrsim k_B T$, but is absent or very weak for $\mu < k_B T$. In the limit $\mu/k_B T \ll 1$, the ratios $\Delta V_{\eta_H}/\Delta V_B$ and $\Delta T_{\eta_H}/\Delta T_B$ become equal and much less than 1 since $n \to 0$ [see Eqs. (7) and (8)]. However, the nonmonotonic behavior of ΔV is different from the one of ΔT due to the Drude contribution in ΔV_B. First, the critical magnetic field for ΔV is smaller than that for ΔT. Second, since σ_Q is small at $\mu \gg k_B T$, the ratio $\Delta T_{\eta_H}/\Delta T_B$ is enhanced and the Hall viscous effect dominates the inverse Nernst effect, which is different for $\Delta V_{\eta_H}/\Delta V_B$ [34].

Suppression of the Lorenz ratio. Our simulations predict a violation of the Wiedemann-Franz law in the Dirac regime which increases with increasing magnetic field and channel width. The Lorenz ratio is

$$L = \frac{\kappa}{\sigma T} = \frac{L_0}{[1 + (n/n_0)^2]^2}, \tag{9}$$

with $L_0 = w v_F^2 \tau_{MR}^{avg}/(T^2 \sigma_Q)$, $n_0^2 = w \sigma_Q/(e^2 v_F^2 \tau_{MR}^{avg})$, and κ the thermal conductivity defined by $Q_x^{avg} = -\kappa \nabla_x T$ at $J_x^{avg} = 0$. The Wiedemann-Franz law $L_{WF} = \pi^2 k_B^2/(3e^2)$ [32], valid for noninteracting systems, was found to be violated for strongly correlated systems [2,59]. As shown in Fig. 3, L implicitly depends on B_z and W via τ_{MR}^{avg}. By increasing W or B_z such that $\tau_{MR}^{avg} \to \tau_{MR}$, L approaches its hydrodynamic form L_∞ in boundaryless graphene.

Conclusion. By considering a channel geometry of graphene subjected to electric and magnetic fields, we have shown that the electronic fluid is characterized by two effective scales due to the finite channel width, i.e., the effective Gurzhi length l_G^{eff} and average momentum relaxation time τ_{MR}^{eff}. The generated Hall voltage in Eq. (7) and temperature gradient in Eq. (8) exhibit a nonmonotonic dependence on the magnetic field that reflects the competition between the Hall viscous and Lorentz effects, where the former is dominant at small and the latter at large magnetic field. Furthermore, one can directly relate the hydrodynamic inverse Nernst signal in the Fermi-liquid regime to its Hall viscous contribution since the Lorentz contribution is suppressed by small σ_Q. Finally, we find that the Lorenz ratio
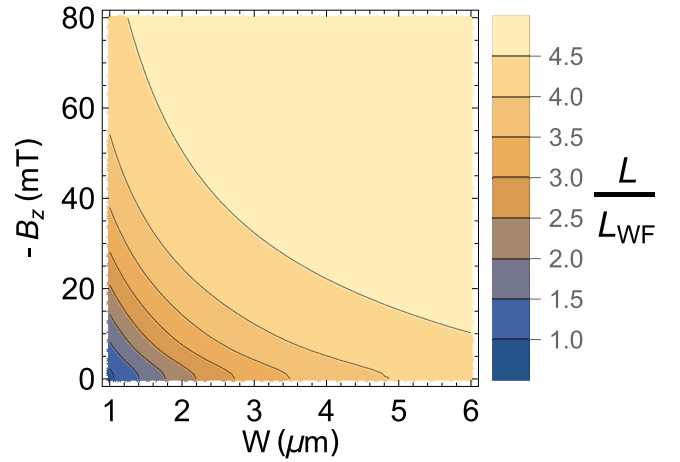

FIG. 3. The Lorenz ratio L in units of L_{WF} as a function of the width W and the magnetic field B_z at $\mu = 0.5 k_B T$ and $T = 120$ K. When $W \to \infty$, it approaches $L_\infty/L_{WF} \approx 4.9$.

in Eq. (9) is suppressed by a finite width W through τ_{MR}^{eff}, while a magnetic field leads to an enhancement of Lorenz ratio. Our results have significant implications for the hydrodynamics of electrons in graphene and we expect them to also be relevant for further strongly coupled hexagonal materials.

Possible extensions of this work include calculating the Hall signal via kinetic theory [60], investigating the effect of out-of-plane magnetic fields and the Hall viscosity on the preturbulent vortex shedding in graphene [61] as well as on fully developed turbulence in kagome metals [62], analyzing the interplay of parity-breaking Hall viscosity with the parity anomaly present, e.g., in quantum anomalous Hall systems [63–65], an analysis of the ac version of the Poiseuille flow [66] including the Hall viscosity, as well as investigating the inverse Nernst effect in multiterminal [7,15] or Corbino geometries [67].

Finally, it was recently suggested that collective effects due to plasmons may also modify thermoelectric transport in graphene [68,69]. The contribution of plasmons to the electrical conductivity and Seebeck coefficient is known to be small without a magnetic field [68]. They mainly affect the thermal conductivity above $\mu/(k_B T) > 1$ and are negligible for the Lorenz ratio considered in Fig. 3 at $B_z = 0$. However, it will be interesting to consider hydrodynamic plasmon dynamics to our results at finite magnetic field in future studies.

[1] P. J. W. Moll, P. Kushwaha, N. Nandi, B. Schmidt, and A. P. Mackenzie, Science **351**, 1061 (2016).

[2] J. Crossno, J. K. Shi, K. Wang, X. Liu, A. Harzheim, A. Lucas, S. Sachdev, P. Kim, T. Taniguchi, K. Watanabe *et al.*, Science **351**, 1058 (2016).

[3] J. A. Sulpizio, L. Ella, A. Rozen, J. Birkbeck, D. J. Perello, D. Dutta, M. Ben-Shalom, T. Taniguchi, K. Watanabe, T. Holder *et al.*, Nature (London) **576**, 75 (2019).

[4] M. J. H. Ku, T. X. Zhou, Q. Li, Y. J. Shin, J. K. Shi, C. Burch, L. E. Anderson, A. T. Pierce, Y. Xie, A. Hamo *et al.*, Nature (London) **583**, 537 (2020).

[5] A. Jenkins, S. Baumann, H. Zhou, S. A. Meynell, Y. Daipeng, K. Watanabe, T. Taniguchi, A. Lucas, A. F. Young, and A. C. Bleszynski Jayich, Phys. Rev. Lett. **129**, 087701 (2022).

[6] U. Vool, A. Hamo, G. Varnavides, Y. Wang, T. X. Zhou, N. Kumar, Y. Dovzhenko, Z. Qiu, C. A. C. Garcia, A. T. Pierce *et al.*, Nat. Phys. **17**, 1216 (2021).

[7] D. Bandurin, I. Torre, R. K. Kumar, M. Ben Shalom, A. Tomadin, A. Principi, G. Auton, E. Khestanova, K. Novoselov, I. Grigorieva *et al.*, Science **351**, 1055 (2016).

[8] P. Gallagher, C.-S. Yang, T. Lyu, F. Tian, R. Kou, H. Zhang, K. Watanabe, T. Taniguchi, and F. Wang, Science **364**, 158 (2019).

[9] A. I. Berdyugin, S. G. Xu, F. M. D. Pellegrino, R. Krishna Kumar, A. Principi, I. Torre, M. Ben Shalom, T. Taniguchi, K. Watanabe, I. V. Grigorieva *et al.*, Science **364**, 162 (2019).

[10] L. Ella, A. Rozen, J. Birkbeck, M. Ben-Shalom, D. Perello, J. Zultak, T. Taniguchi, K. Watanabe, A. K. Geim, S. Ilani *et al.*, Nat. Nanotechnol. **14**, 480 (2019).

[11] D. A. Bandurin, A. V. Shytov, L. S. Levitov, R. K. Kumar, A. I. Berdyugin, M. Ben Shalom, I. V. Grigorieva, A. K. Geim, and G. Falkovich, Nat. Commun. **9**, 4533 (2018).

[12] A. Lucas and K. Chung Fong, J. Phys.: Condens. Matter **30**, 053001 (2018).

[13] B. N. Narozhny, I. V. Gornyi, A. D. Mirlin, and J. Schmalian, Ann. Phys. **529**, 1700043 (2017).

[14] B. N. Narozhny, Riv. Nuovo Cimento **45**, 661 (2022).

[15] I. Torre, A. Tomadin, A. K. Geim, and M. Polini, Phys. Rev. B **92**, 165433 (2015).

[16] L. W. Molenkamp and M. J. M. de Jong, Phys. Rev. B **49**, 5038 (1994).

[17] M. J. M. de Jong and L. W. Molenkamp, Phys. Rev. B **51**, 13389 (1995).

[18] G. Gusev, A. Levin, E. Levinson, and A. Bakarov, AIP Adv. **8**, 025318 (2018).

[19] P. S. Alekseev, Phys. Rev. Lett. **117**, 166601 (2016).

[20] P. S. Alekseev, A. P. Dmitriev, I. V. Gornyi, V. Y. Kachorovskii, B. N. Narozhny, M. Schütt, and M. Titov, Phys. Rev. Lett. **114**, 156601 (2015).

[21] P. S. Alekseev, A. P. Dmitriev, I. V. Gornyi, V. Y. Kachorovskii, B. N. Narozhny, and M. Titov, Phys. Rev. B **97**, 085109 (2018).

[22] P. S. Alekseev, A. P. Dmitriev, I. V. Gornyi, V. Y. Kachorovskii, B. N. Narozhny, M. Schütt, and M. Titov, Phys. Rev. B **95**, 165410 (2017).

[23] J. E. Avron, R. Seiler, and P. G. Zograf, Phys. Rev. Lett. **75**, 697 (1995).

[24] K. Jensen, M. Kaminski, P. Kovtun, R. Meyer, A. Ritz, and A. Yarom, J. High Energy Phys. 05 (2012) 102.

[25] C. Hoyos, Int. J. Mod. Phys. B **28**, 1430007 (2014).

[26] I. Matthaiakakis, D. Rodríguez Fernández, C. Tutschku, E. M. Hankiewicz, J. Erdmenger, and R. Meyer, Phys. Rev. B **101**, 045423 (2020).

[27] Note that we are prohibited from going to arbitrarily small densities since charge puddles are present in graphene [12].

[28] M. Müller, L. Fritz, and S. Sachdev, Phys. Rev. B **78**, 115406 (2008).

[29] K. Behnia and H. Aubin, Rep. Prog. Phys. **79**, 046502 (2016).

[30] A. Sakai, Y. P. Mizuta, A. A. Nugroho, R. Sihombing, T. Koretsune, M.-T. Suzuki, N. Takemori, R. Ishii, D. Nishio-Hamane, R. Arita *et al.*, Nat. Phys. **14**, 1119 (2018).

[31] D. G. Rothe, E. M. Hankiewicz, B. Trauzettel, and M. Guigou, Phys. Rev. B **86**, 165434 (2012).

[32] R. Franz and G. Wiedemann, Ann. Phys. Chem. **165**, 497 (1853).

[33] N. W. Ashcroft and N. D. Mermin, *Solid State Physics* (Holt, Rinehart and Winston, New York, 1976).

[34] See Supplemental Material at http://link.aps.org/supplemental/10.1103/PhysRevB.107.L201403 for details on the calculations, momentum, and energy relaxation, the analytic solutions to the linearized Navier-Stokes equations, and complementary figures of the Hall response, which includes Refs. [35,70–76].

[35] J. Avron, J. Stat. Phys. **92**, 543 (1998).

[36] Bulk viscous effects are negligible in graphene, at least to leading order [48,77,78].

[37] We will not approach the charge neutrality point at which the imbalance current and the recombination of electrons and holes becomes important [48].

[38] E. H. Hwang and S. Das Sarma, Phys. Rev. B **77**, 115449 (2008).

[39] D. K. Efetov and P. Kim, Phys. Rev. Lett. **105**, 256805 (2010).

[40] S. Adam, E. H. Hwang, V. M. Galitski, and S. D. Sarma, Proc. Natl. Acad. Sci. USA **104**, 18392 (2007).

[41] R. Bistritzer and A. H. MacDonald, Phys. Rev. Lett. **102**, 206410 (2009).

[42] W.-K. Tse and S. Das Sarma, Phys. Rev. B **79**, 235406 (2009).

[43] B. Narozhny and I. Gornyi, Front. Phys. **9**, 640649 (2021).

[44] J. C. W. Song, M. Y. Reizer, and L. S. Levitov, Phys. Rev. Lett. **109**, 106602 (2012).

[45] M. W. Graham, S.-F. Shi, D. C. Ralph, J. Park, and P. L. McEuen, Nat. Phys. **9**, 103 (2013).

[46] A. C. Betz, S. H. Jhang, E. Pallecchi, R. Ferreira, G. Fève, J. M. Berroir, and B. Plaçais, Nat. Phys. **9**, 109 (2013).

[47] K. C. Fong, E. E. Wollman, H. Ravi, W. Chen, A. A. Clerk, M. D. Shaw, H. G. Leduc, and K. C. Schwab, Phys. Rev. X **3**, 041008 (2013).

[48] B. N. Narozhny, Ann. Phys. **411**, 167979 (2019).

[49] L. D. Landau and E. M. Lifshitz, *Fluid Mechanics: Course of Theoretical Physics*, (Elsevier, Amsterdam, 2013), Vol. 6.

[50] S. A. Hartnoll, P. K. Kovtun, M. Muller, and S. Sachdev, Phys. Rev. B **76**, 144502 (2007).

[51] The nonlocal Coulomb interactions could break Lorentz invariance at second order in the velocities [12].

[52] B. N. Narozhny and M. Schütt, Phys. Rev. B **100**, 035125 (2019).

[53] L. Fritz, J. Schmalian, M. Müller, and S. Sachdev, Phys. Rev. B **78**, 085416 (2008).

[54] E. I. Kiselev and J. Schmalian, Phys. Rev. B **99**, 035430 (2019).

[55] R. N. Gurzhi, Sov. Phys. JETP **44**, 771 (1963).

[56] R. N. Gurzhi, Sov. Phys. Usp. **11**, 255 (1968).

[57] J. Erdmenger, I. Matthaiakakis, R. Meyer, and D. R. Fernández, Phys. Rev. B **98**, 195143 (2018).

[58] M. Müller and S. Sachdev, Phys. Rev. B **78**, 115419 (2008).

[59] R. Mahajan, M. Barkeshli, and S. A. Hartnoll, Phys. Rev. B **88**, 125107 (2013).

[60] T. Scaffidi, N. Nandi, B. Schmidt, A. P. Mackenzie, and J. E. Moore, Phys. Rev. Lett. **118**, 226601 (2017).

[61] M. Mendoza, H. J. Herrmann, and S. Succi, Phys. Rev. Lett. **106**, 156601 (2011).

[62] D. Di Sante, J. Erdmenger, M. Greiter, I. Matthaiakakis, R. Meyer, D. Rodríguez Fernández, R. Thomale, E. van Loon, and T. Wehling, Nat. Commun. **11**, 3997 (2020).

[63] J. Böttcher, C. Tutschku, L. W. Molenkamp, and E. M. Hankiewicz, Phys. Rev. Lett. **123**, 226602 (2019).

[64] C. Tutschku, J. Böttcher, R. Meyer, and E. M. Hankiewicz, Phys. Rev. Res. **2**, 033193 (2020).

[65] C. Tutschku, F. S. Nogueira, C. Northe, J. van den Brink, and E. M. Hankiewicz, Phys. Rev. B **102**, 205407 (2020).

[66] R. Moessner, P. Surówka, and P. Witkowski, Phys. Rev. B **97**, 161112(R) (2018).

[67] T. Holder, R. Queiroz, and A. Stern, Phys. Rev. Lett. **123**, 106801 (2019).

[68] K. Pongsangangan, T. Ludwig, H. T. C. Stoof, and L. Fritz, Phys. Rev. B **106**, 205126 (2022).

[69] K. Pongsangangan, T. Ludwig, H. T. C. Stoof, and L. Fritz, Phys. Rev. B **106**, 205127 (2022).

[70] A. H. Castro Neto, F. Guinea, N. M. R. Peres, K. S. Novoselov, and A. K. Geim, Rev. Mod. Phys. **81**, 109 (2009).

[71] K. S. Novoselov, A. K. Geim, S. V. Morozov, D. Jiang, M. I. Katsnelson, I. Grigorieva, S. V. Dubonos, and A. A. Firsov, Nature (London) **438**, 197 (2005).

[72] B. N. Narozhny, M. Titov, I. V. Gornyi, and P. M. Ostrovsky, Phys. Rev. B **85**, 195421 (2012).

[73] D. E. Sheehy and J. Schmalian, Phys. Rev. Lett. **99**, 226803 (2007).

[74] Y. Zhang, Y.-W. Tan, H. L. Stormer, and P. Kim, Nature (London) **438**, 201 (2005).

[75] E. H. Hwang and S. Das Sarma, Phys. Rev. B **75**, 205418 (2007).

[76] J. H. Strait, H. Wang, S. Shivaraman, V. Shields, M. Spencer, and F. Rana, Nano Lett. **11**, 4902 (2011).

[77] M. Müller, J. Schmalian, and L. Fritz, Phys. Rev. Lett. **103**, 025301 (2009).

[78] U. Briskot, M. Schütt, I. V. Gornyi, M. Titov, B. N. Narozhny, and A. D. Mirlin, Phys. Rev. B **92**, 115426 (2015).